Geometric Constraint-based Reconfiguration and Self-motions of a 4-CRU Parallel Mechanism

Latifah Nurahmi[1]*, **Pradiktio Putrayudanto**[1], **Guowu Wei**[2], **Sunil K. Agrawal**[3]

[1]Department of Mechanical Engineering, Institut Teknologi Sepuluh Nopember
Kampus ITS Sukolilo, 60111, Surabaya, Indonesia
Emails: latifah.nurahmi@me.its.ac.id, pradiktio.putrayudanto16@mhs.me.its.ac.id
[2]School of Science, Engineering and Environment, Salford University, Salford, M5 4WT, United Kingdom
Email: g.wei@salford.ac.uk
[3]Department of Mechanical Engineering, Columbia University, New York, NY 10027 USA
Email: sunil.agrawal@columbia.edu

ABSTRACT

Over the past few years, the concept of multi-directional 3D printing has been introduced to print complex shapes and overhang geometry. This technique requires the nozzle to constantly change orientation to print the object along its tangential direction. A 6-DOF (Degree-Of-Freedom) robotic arm or Stewart platform can be a solution, but these mechanisms use more components and motors. An alternative solution has been proposed in this paper based on a 4-CRU mechanism. This mechanism can orient the nozzle by switching into different motion types with minimal numbers of motors while keeping the mechanism rigid and agile. Therefore, analyses of the reconfiguration, workspace, singularities, and self-motions of a 4-CRU mechanism presented in this paper have become necessities. By using primary decomposition, four geometric constraints have been identified, and the reconfiguration analysis has been carried out in each of these. It reveals that each geometric constraint will have three distinct operation modes, namely Schönflies mode, reversed Schönflies mode, and an additional mode. The additional mode can either be a 4-DOF mode or a degenerated 3-DOF mode, depending on the type of geometric constraints. By taking into account the actuation and constraint singularities, the workspace of each operation mode has been analysed and geometrically illustrated. It allows us to determine the regions in which the reconfiguration takes place. Furthermore, the inherent self-motion in the Schönflies mode is revealed and illustrated, which occurs at two specified actuated leg lengths. Demonstration of the reconfiguration process and self-motions are provided through a mock-up prototype.

1 Introduction

Over the past few decades, investigations on reconfigurable mechanisms have been carried out under different terms, e.g., kinematotropic mechanisms [1,2], metamorphic mechanisms [3,4,5], deployable mechanisms [6,7,8], and mechanisms with multiple operation modes [9,10]. The concept of operation modes was initially developed to drive attention to interpret five distinct 3-DOF motions performed by the DYMO (Double Y-Multi Operational) [11]. Based on Euler-Quaternion parameters, types of operation modes and transition configurations were investigated in [12,13]. The Study's kinematic mapping and algebraic geometry approach were used to reveal the Schönflies mode and reversed Schönflies mode of the 4-RUU and 2-RUU parallel mechanisms [14,15]. Later, the translational parts of the Study's kinematic mapping were modified to identify the workspace transition of the 3-(rR)PS metamorphic parallel mechanism [16,17]. The same method was employed in [18] to synthesize the design parameters for medical purposes [19,20,21]. The Cayley parametrization was implemented in [22] to determine several extra modes of the 4-UPU parallel mechanism.

The reconfiguration process from one operation mode to another involves a constraint singularity. The conditions for switching the operation modes of a 3-PRPiR parallel robot involving lockable Pi (parallelogram) and R joints were investigated in [23]. A systematic approach was proposed in [24] to synthesize multi-modes manipulators with lockable-joints such

---

*Corresponding author

that constraint singularities can be avoided during reconfiguration. In [25], brakes and timing belts were installed in the DI-RECTOR (DIsassembly-free REConfigurable parallel manipulaTOR) to enable passage through the constraint singularities. A reconfigurable platform is also a solution for the mechanisms to switch the operation modes without crossing constraint singularities. A special case of singularity may occur where the moving-platform can perform continuous and finite motions when all actuators are locked. This class of singularity is called *self-motions* [26, 27].

Serial and parallel mechanisms have been used for 3D-printing technology for building construction, which is currently being explored by many researchers. 3D-printing technology offers many advantages compared to conventional construction processes, such as reduced waste and cost, operation time saving and the ability to generate complex architectures. An important application is contour crafting [28], which is a computerized additive manufacturing technology that uses trowels to build a polished planar and free form surface. A D-shape project was started by Cesaretti *et. al.* [29] which used a binding agent and special powder as the two main components of the deposited material. A gantry mechanism was applied to both the contour crafting and D-shape building construction projects.

For such printing mechanisms, the nozzle moves in limited X, Y, and Z linear motions without orientation functionality. The printabilities of those mechanisms are quite poor when it comes to printing complex shapes or overhang geometry, for example the tilted wall in Fig. 1. As a consequence, additional support is needed to prevent the concrete mixture from collapsing due to gravity. It becomes less efficient, lengthens the printing process, and reduces its flexibility. Furthermore, the final result is lacking in surface quality due to stair-stepping effects, as shown in Fig. 1.

Several researchers have attempted to overcome these issues by introducing the idea of a multi-directional 3D printing process where the nozzle can be freely oriented to print the workpiece along its tangential direction, as shown in Fig. 1. Krejcirik *et al.* [30] applied a 6-DOF robotic arm to print overhang geometry without support. This strategy enables higher bonding quality than the gravitational force due to the self-supportive fiber deposition. Although the robotic arm can be designed to follow complex trajectories, the nozzle and extruder, which should be carried by the moving-platform, will increase the base motor loads and decrease its agility.
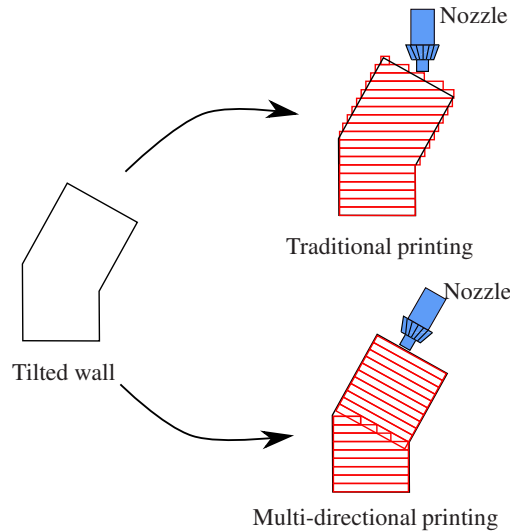

Fig. 1: Illustration of traditional and multi-directional 3D printing

If compared to serial robotic arms, parallel mechanisms use several short chains and are intrinsically more robust to unwanted movements. A Stewart mechanism was employed in [31] to create a low-cost additive manufacturing with multi-directional deposition process. All six motors were mounted on top of the frame, leading to vibrations. Instead of using extra motors for extra DOF, Gao *et al.* [32] operated a 5-DOF Computer Numerical Control (CNC) to minimize the use of supportive material. The base-platform carrying the workpiece moves in two rotational axes in addition to 3-DOF linear motions of the print head. This method cannot be adopted for printing big and heavy parts, such as buildings or houses.

Motivated by those problems, we developed a 4-CRU[1] mechanism for 3D printing buildings. This mechanism is able to reconfigure beyond its original 4-DOF motions. By reconfiguring, the nozzle carried by the platform can switch into different motion types, hence the nozzle can print the workpiece along its tangential direction, as shown in Fig. 1. The reconfiguration is very useful for this application since we perform more motion types with less parts and motors as compared to the Stewart platform. All actuators of the 4-CRU mechanism are fixed on the ground, which will enable the mechanism to be more rigid

---

[1]C, R, U stand for cylindrical, revolute, universal joint.

and agile, as compared to the serial robotic arm. Since we aim to print large parts, such as buildings, the ground carrying the workpiece cannot be oriented. This contrasts with the 5-DOF CNC, and all orientation functions should be conducted by the platform via reconfiguration.

Accordingly, this paper focuses on the analysis of reconfiguration, workspace, singularities and self-motions of a 4-CRU parallel mechanism with the change of its geometric constraints. The rest of this paper is organized as follows: the application of a 4-CRU parallel mechanism for 3D-printing building is briefly explained in Section 2. Section 3 provides the mechanism description and the derivation of constraint equations. The primary decomposition is computed as a set of constraint equations to determine the number and types of operation modes in Section 4. The workspace and actuation singularities for different operation modes are presented in Sections 5. The reconfiguration between operation modes is described in Section 6 and the self-motions are analysed and demonstrated in Section 7. Eventually, conclusions for this research are addressed in Section 8.

2 Application for 3D-Printing Building

3D-printing technology has continued to grow since its emergence. This technology can be used to create simple parts or complex building shapes. The process of printing a building is carried out by a super-sized printer which deposits a special concrete and composite mixture in layers. This mixture is much thicker than regular construction concrete.

A 4-CRU parallel mechanism performing 4-DOF motions (three translations about X, Y, Z directions and one rotation about Z axis) is proposed as a 3D printing buildings, as shown in Fig. 2. This mechanism is composed of four identical CRU legs in which each leg is actuated by one linear motor. All linear motors are vertically fixed on the ground, which will make the mechanism lighter and more agile when executing a printing task. Thanks to its structure, the load carried by the moving-platform can be evenly distributed to all four CRU legs. In addition to 4-DOF motions, the mechanism is able to reconfigure its motion types continuously into several distinct 3-DOF motions. Each motion type corresponds to a specific operation mode.

As stated in Section 1, a 4-CRU parallel mechanism is used to accomplish multi-configuration printing where the print head motions can be continuously reconfigured in multiple axes without extra motors. Therefore, the reconfiguration ability is the main interest of this paper. The influences of geometric constraints to the changes in operation modes are explored. The constraint singularities between operation modes are characterized, so we can detect the regions in which the reconfiguration takes place.

Fig. 2: Application for a 3D-printing buildings

3 Mechanism Description and Constraint Equations
3.1 Mechanism Description

The structure of a 4-CRU parallel mechanism is shown in Fig. 3. This mechanism is composed of a reconfigurable base and moving-platform, which are connected by four identical legs. Each leg is connected to the reconfigurable base and the moving-platform by a cylindrical joint, a revolute joint, and a universal joint. The fixed frame Σ_0 is defined by the origin O

of coordinates x, y, z and located at the center of base. The moving-frame Σ_1 is defined by the origin P of coordinates u, v, w and located at the center of moving-platform.

In each leg, the cylindrical and revolute joints are built with perpendicular and intersecting axes. The cylindrical joint of each leg is attached to the base and its translational motion is actuated along the axis $\mathbf{s}_i$, where $i = 1, .., 4$. Its unit vector expressed in the fixed frame is defined as: $\mathbf{s}_i^0 = \begin{bmatrix} 0 & 0 & 1 \end{bmatrix}^T$. The linear distance h_i of the cylindrical joint is the actuated leg length which is measured from point A_i to B_i, as shown in Fig. 4. The base is bounded by four vertices A_i. The length a is defined from origin O of the fixed frame to the mid-edges of A_1A_2 and A_3A_4, as shown in Fig. 5. Likewise, length b is defined from the origin O of the fixed frame to the mid-edges of A_2A_3 and A_4A_1. The revolute joint of leg i is located at point B_i. The coordinates of point B_i expressed in the fixed frame are:

$$
\begin{aligned}
\mathbf{b}_1^0 &= \begin{bmatrix} a & -b & h_1 \end{bmatrix}^T & \mathbf{b}_2^0 &= \begin{bmatrix} a & b & h_2 \end{bmatrix}^T \\
\mathbf{b}_3^0 &= \begin{bmatrix} -a & b & h_3 \end{bmatrix}^T & \mathbf{b}_4^0 &= \begin{bmatrix} -a & -b & h_4 \end{bmatrix}^T
\end{aligned}
\tag{1}
$$

The moving-platform is bounded by four universal joints, of which the intersection point of the revolute joints is denoted by point C_i. The first and second joints of the universal joint are directed along the axes $\mathbf{m}_i$ and $\mathbf{n}_i$, respectively. The unit vector of $\mathbf{n}_i$ expressed in the moving-frame is defined as: $\mathbf{n}_i^1 = \begin{bmatrix} 0 & 0 & 1 \end{bmatrix}^T$. The length of segment B_iC_i is denoted by r. The length c is defined from the origin P of the moving-frame to the mid-edges of C_1C_2 and C_3C_4, as shown in Fig. 5. Likewise, the length d is defined from the origin P of the fixed frame to the mid-edges of C_2C_3 and C_4C_1. The coordinates of point C_i expressed in the moving-frame are:

$$
\begin{aligned}
\mathbf{c}_1^1 &= \begin{bmatrix} c & -d & 0 \end{bmatrix}^T & \mathbf{c}_2^1 &= \begin{bmatrix} c & d & 0 \end{bmatrix}^T \\
\mathbf{c}_3^1 &= \begin{bmatrix} -c & d & 0 \end{bmatrix}^T & \mathbf{c}_4^1 &= \begin{bmatrix} -c & -d & 0 \end{bmatrix}^T
\end{aligned}
\tag{2}
$$

As the base and moving-platform are reconfigurable, the lengths $a, b, c,$ and d can be assigned with arbitrary values. In the following, the number and types of operation modes and the singularity conditions are investigated for different values of design parameters a, b, c, d.
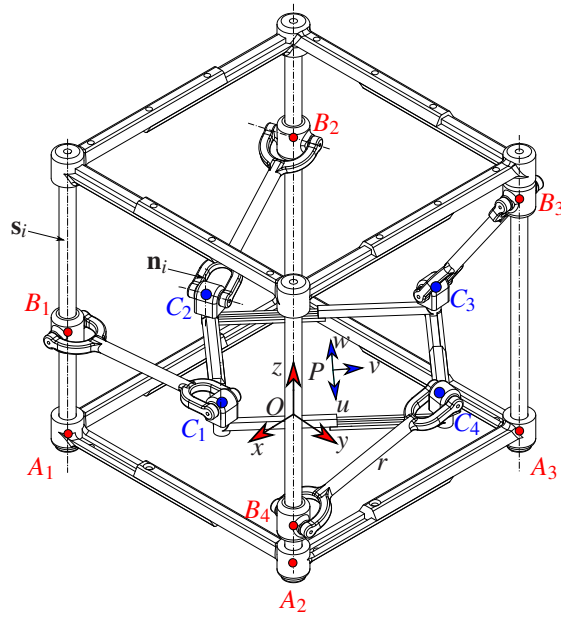

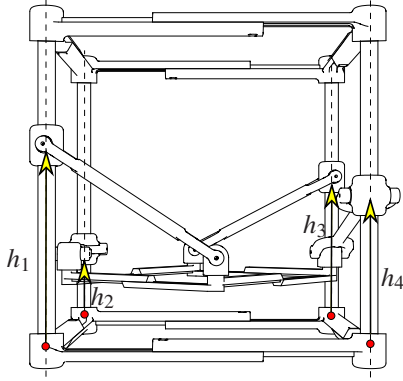Fig. 3: Isometric view of a 4-CRU parallel mechanism

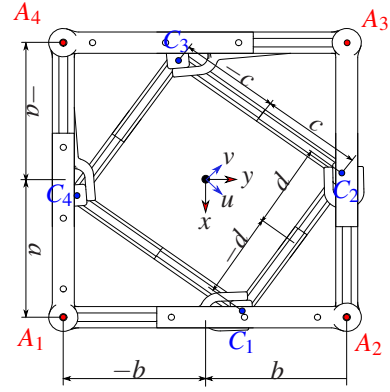Fig. 4: Front view of a 4-CRU parallel mechanism

Fig. 5: Top view of a 4-CRU parallel mechanism

3.2   Constraint Equations

The initial step in deriving the constraint equations is to perform the coordinate transformation of the moving-platform vertices C_i and the unit vectors $\mathbf{n}_i$. The Quaternion parameters x_0, x_1, x_2, x_3 and point-displacement X, Y, Z are used and formulated to be rotation matrix $\mathbf{R}$ and displacement vector $\mathbf{d}$, respectively. Both matrix $\mathbf{R}$ and vector $\mathbf{d}$ are combined to be a homogeneous transformation matrix $\mathbf{T}$, as follows:

$$\mathbf{R} = \begin{pmatrix} x_0^2 + x_1^2 - x_2^2 - x_3^2 & 2(x_1x_2 - x_0x_3) & 2(x_1x_3 + x_0x_2) \\ 2(x_1x_2 + x_0x_3) & x_0^2 - x_1^2 + x_2^2 - x_3^2 & 2(x_2x_3 - x_0x_1) \\ 2(x_1x_3 - x_0x_2) & 2(x_2x_3 + x_0x_1) & x_0^2 - x_1^2 - x_2^2 + x_3^2 \end{pmatrix}, \quad \mathbf{d} = \begin{pmatrix} X \\ Y \\ Z \end{pmatrix}, \quad \mathbf{T} = \begin{pmatrix} \mathbf{R} & \mathbf{d} \\ \mathbf{0}_{1\times 3} & 1 \end{pmatrix} \quad (3)$$

All those seven parameters are useful in representing the spatial displacement of a rigid body. Then, the coordinates of points C_i and unit vectors $\mathbf{n}_i$ expressed in the fixed-frame can be determined through transformation, namely:

$$\mathbf{c}_i^0 = \mathbf{R}\,\mathbf{c}_i^1 + \mathbf{d}, \quad i = 1, .., 4$$
$$\mathbf{n}_i^0 = \mathbf{R}\,\mathbf{n}_i^1, \quad i = 1, .., 4 \quad (4)$$

Once all coordinates of points and unit vectors are expressed in terms of Euler-Quaternion parameters, the constraint equations can be derived by examining the geometric conditions of each CRU leg. The link connecting points B_i to C_i can be defined by a vector:

$$\mathbf{u}_i^0 = \mathbf{c}_i^0 - \mathbf{b}_i^0 \quad i = 1, .., 4 \quad (5)$$

Vector $\mathbf{u}_i$ is always coplanar to the unit vectors $\mathbf{s}_i$ and $\mathbf{n}_i$, as shown in Fig. 6. This condition can be mathematically formulated as a scalar triple product, as follows:

$$(\mathbf{s}_i^0 \times \mathbf{n}_i^0)^T \mathbf{u}_i^0 = 0, \quad i = 1, .., 4 \quad (6)$$

By applying Eq. (6) to all CRU legs, four constraint equations can be determined as follows:

$$\begin{aligned} f_1 &: Xx_0x_1 - Xx_2x_3 + Yx_0x_2 + Yx_1x_3 - ax_0x_1 + ax_2x_3 + bx_0x_2 + bx_1x_3 + cx_0x_1 + cx_2x_3 - dx_0x_2 + dx_1x_3 = 0 \\ f_2 &: Xx_0x_1 - Xx_2x_3 + Yx_0x_2 + Yx_1x_3 - ax_0x_1 + ax_2x_3 - bx_0x_2 - bx_1x_3 + cx_0x_1 + cx_2x_3 + dx_0x_2 - dx_1x_3 = 0 \\ f_3 &: Xx_0x_1 - Xx_2x_3 + Yx_0x_2 + Yx_1x_3 + ax_0x_1 - ax_2x_3 - bx_0x_2 - bx_1x_3 - cx_0x_1 - cx_2x_3 + dx_0x_2 - dx_1x_3 = 0 \\ f_4 &: Xx_0x_1 - Xx_2x_3 + Yx_0x_2 + Yx_1x_3 + ax_0x_1 - ax_2x_3 + bx_0x_2 + bx_1x_3 - cx_0x_1 - cx_2x_3 - dx_0x_2 + dx_1x_3 = 0 \end{aligned} \quad (7)$$
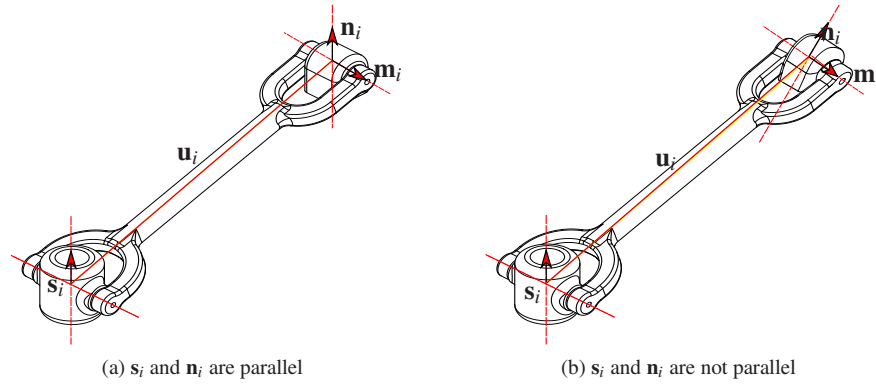
(a) $\mathbf{s}_i$ and $\mathbf{n}_i$ are parallel   (b) $\mathbf{s}_i$ and $\mathbf{n}_i$ are not parallel

Fig. 6: Geometric condition of the CRU leg

Let the linear motions h_1, h_2, h_3, h_4 of C-joint in CRU legs be actuated. The length of link B_iC_i is defined by r. It follows that point C_i can move along a circle of point B_i and radius r, which is mathematically defined as follows: $\| \mathbf{c}_i^0 - \mathbf{b}_i^0 \|^2 = r^2$. This computation yields:

$$
\begin{aligned}
f_5 : \ & -4d(Y+b)x_2^2 + 4c(X-a)x_1^2 + 4c(Z-h_1)x_1x_3 - 4d(Z-h_1)x_2x_3 - 4d(Z-h_1)x_0x_1 - 4c(Z-h_1)x_0x_2 + (4Xc \\
& -4Yd - 4ac - 4bd)x_0^2 - 2h_1Z + (4Xd + 4Yc - 4ad + 4bc)x_0x_3 + (-4Xd + 4Yc + 4ad + 4bc)x_1x_2 + 2Yb + Z^2 \\
& + h_1^2 - r^2 - 2Xa - 2Xc + Y^2 + X^2 + c^2 + 2dY + a^2 + b^2 + d^2 + 2ac + 2bd = 0 \\
f_6 : \ & 4c(X-a)x_1^2 + 4d(Y-b)x_2^2 + (4Xd + 4Yc - 4ad - 4bc)x_1x_2 + (-4Xd + 4Yc + 4ad - 4bc)x_0x_3 + (4Xc + 4Yd \\
& -4ac - 4bd)x_0^2 + h_2^2 - 2h_2Z - 2Yb + Z^2 - r^2 - 2Xa - 2Xc + 4d(Z-h_2)x_0x_1 - 4c(Z-h_2)x_0x_2 + 4c(Z-h_2) \\
& x_1x_3 + 4d(Z-h_2)x_2x_3 + Y^2 + X^2 + c^2 - 2dY + a^2 + b^2 + d^2 + 2ac + 2bd = 0 \\
f_7 : \ & 4d(Y-b)x_2^2 - 4c(X+a)x_1^2 + (-4Xd - 4Yc - 4ad + 4bc)x_0x_3 + (4Xd - 4Yc + 4ad + 4bc)x_1x_2 + (-4Xc + 4 \\
& Yd - 4ac - 4bd)x_0^2 - 2h_3Z + h_3^2 - 2Yb + Z^2 - r^2 + 2Xa + 2Xc - 4c(Z-h_3)x_1x_3 + 4c(Z-h_3)x_2x_0 + 4d(Z- \\
& h_3)x_1x_0 + 4d(Z-h_3)x_2x_3 + Y^2 + X^2 + c^2 - 2dY + a^2 + b^2 + d^2 + 2ac + 2bd = 0 \\
f_8 : \ & -4c(X+a)x_1^2 + (-4Xd - 4Yc - 4ad - 4bc)x_1x_2 + (4Xd - 4Yc + 4ad - 4bc)x_0x_3 - 2Zh_4 + (-4Xc - 4Yd - \\
& 4ac - 4bd)x_0^2 + h_4^2 + 2Yb + Z^2 - r^2 + 2Xa + 2Xc + Y^2 + X^2 - 4d(Y+b)x_2^2 + c^2 + 2dY + a^2 + b^2 + d^2 + 2ac \\
& + 2bd + 4c(Z-h_4)x_2x_0 - 4d(Z-h_4)x_1x_0 - 4d(Z-h_4)x_2x_3 - 4c(Z-h_4)x_1x_3 = 0
\end{aligned}
\tag{8}
$$

The norm of Quaternion parameters is computed and when its norm is equal to 1, the Quaternion parameters are called normalized Quaternions. This normalization equation is added to be the ninth constraint equation, as follows:

$$
f_9 : \ x_0^2 + x_1^2 + x_2^2 + x_3^2 - 1 = 0
\tag{9}
$$

Eq. (9) should be fulfilled which means that $x_0 = x_1 = x_2 = x_3 = 0$ should be excluded. In the following, all constraint equations were examined to determine the number and types of operation modes.

4   Description of Operation Modes

It is well known that design parameters have great influence on the numbers and types of operation modes. The conditions of design parameters $a, b, c,$ and d and their effects on the numbers and types of operation modes of the 4-CRU parallel mechanism will be analyzed hereafter.

The solutions of nine equations $f_1, f_2, f_3, f_4, f_5, f_6, f_7, f_8, f_9$ will be the solutions of direct kinematics. A polynomial ideal that consists of four polynomials is formulated to analyze the operation modes, i.e. $\mathcal{H} = \langle f_1, f_2, f_3, f_4 \rangle$. This ideal is independent of the actuated lengths h_1, h_2, h_3, h_4 and it is defined by parameters $(x_0, x_1, x_2, x_3, X, Y)$ and coefficient ring $\mathbb{C}[a, b, c, d, r]$. The primary decomposition is computed over the ideal $\mathcal{H}$ to identify if the ideal $\mathcal{H}$ is the intersection of

several sub-ideals. Indeed, the primary decomposition returns several sub-ideals, such that:

$$\mathcal{H} = \bigcap_{j=1}^{3} \mathcal{H}_j \tag{10}$$

The results of sub-ideals $\mathcal{H}_j$ are as follows:

$$\mathcal{H}_1 : \langle x_1, x_2 \rangle$$
$$\mathcal{H}_2 : \langle x_0, x_3 \rangle$$
$$\mathcal{H}_3 : \langle (b^2c^2 - c^2d^2)X^2 + (a^2d^2 - c^2d^2)Y^2, (ab - ad - bc + cd)x_0^2 + (ab + ad + bc + cd)x_3^2, (ab + ad - bc - cd)x_1^2 \tag{11}$$
$$+ (ab - ad + bc - cd)x_2^2, (a - c)x_0x_1 + (-a - c)x_2x_3, (b - d)x_0x_2 - (a + c)x_1x_3, (-ad + cd)Yx_1 + (bc - c$$
$$d)Xx_2, (ad - cd)Yx_0 + (bc + cd)Xx_3, (bc - cd)Xx_0 - (ad + cd)Yx_3, (bc + cd)Xx_1 + (ad + cd)Yx_2 \rangle$$

The sub-ideals $\mathcal{H}_j$ do not contain any other sub-ideals, which means that the sub-ideals $\mathcal{H}_j$ are prime ideals. The prime ideals $\mathcal{H}_j$ define the types of operation modes that belong to the studied 4-CRU parallel mechanism. The first and second sub-ideals, $\mathcal{H}_1$ and $\mathcal{H}_2$, correspond to the 4-DOF operation modes, namely the Schönflies mode and reversed Schönflies mode, respectively. Each operation mode will be discussed in the following sub-sections.

4.1 Operation Mode 1: Schönflies Mode ($\mathcal{H}_1$)

The first operation mode is named Schönflies mode which is described by the condition $x_1 = 0$ and $x_2 = 0$. This condition is valid for all poses and is substituted into the transformation matrix **T**, which yields:

$$\mathbf{T}_{\mathcal{H}_1} = \begin{pmatrix} x_0^2 - x_3^2 & 2x_0x_3 & 0 & X \\ 2x_0x_3 & x_3^2 - x_0^2 & 0 & Y \\ 0 & 0 & 1 & Z \\ 0 & 0 & 0 & 1 \end{pmatrix} \tag{12}$$

The transformation matrix $\mathbf{T}_{\mathcal{H}_1}$ specifies that the moving-platform has 4-DOF motions. This motion is composed of 3-DOF translational motions defined by the parameters X, Y, Z and 1-DOF rotational motion about the positive z-axis of the fixed frame Σ_0. The rotational motion is parametrized by x_0 and x_3 which should simultaneously satisfy the normalization equation defined in Eq. (9).

The Jacobian matrix of the Schönflies mode can be formulated based on the Screw theory. In this operation mode, the axis $\mathbf{n}_i$ is always pointing upward and parallel to the axis $\mathbf{s}_i$ as shown in Fig. 6(a). Each has one constraint screw that is reciprocal to all five twists of CRU leg. This constraint screw can be described intuitively as an infinite-pitch screw which is perpendicular to the axes $\mathbf{m}_i$ and $\mathbf{n}_i$ on the moving-platform (Fig. 6(a)), as: $\hat{\$}_{ci} = \begin{bmatrix} \mathbf{0} \\ \mathbf{m}_i \times \mathbf{n}_i \end{bmatrix}$. Since four constraint screws, $\hat{\$}_{ci}$, geometrically lie in the same horizontal plane of moving-platform, the constraint screws in non-singular configuration is 2-system. It means that two arbitrary constraint screws, e.g. $\hat{\$}_{c1}, \hat{\$}_{c2}$, can be selected to be the Jacobian of the constraint, as follows:

$$\mathbf{J}_{\mathcal{H}_{1c}} = \begin{bmatrix} (\mathbf{m}_1 \times \mathbf{n}_1)^T & \mathbf{0}_{1\times 3} \\ (\mathbf{m}_2 \times \mathbf{n}_2)^T & \mathbf{0}_{1\times 3} \end{bmatrix} \tag{13}$$

By considering that the translational motion of C-joint of CRU leg is actuated, each leg has one additional screw that is reciprocal to all except the translational screw within the CRU leg. This is a zero-pitch screw whose axis is along vector $\mathbf{u}_i$, as follows: $\hat{\$}_{ai} = \begin{bmatrix} \mathbf{u}_i \\ \mathbf{c}_i^0 \times \mathbf{u}_i \end{bmatrix}$. On taking the reciprocal product of this zero-pitch screw with the moving-platform twist and the screws representing the CRU joints within the i-th leg, one can solve for the translational rate of the C-joint and the

moving-platform rates. In non-singular configuration, the actuation screws in this mode form the 4-system of Jacobian of actuation, as follows:

$$\mathbf{J}_{\mathcal{H}_{1a}} = \begin{bmatrix} (\mathbf{c}_1^0 \times \mathbf{u}_1)^T & \mathbf{u}_1^T \\ (\mathbf{c}_2^0 \times \mathbf{u}_2)^T & \mathbf{u}_2^T \\ (\mathbf{c}_3^0 \times \mathbf{u}_3)^T & \mathbf{u}_3^T \\ (\mathbf{c}_4^0 \times \mathbf{u}_4)^T & \mathbf{u}_4^T \end{bmatrix} \tag{14}$$

As a consequence, we define the Jacobian matrix to comprise the 4-system of $\mathbf{J}_{\mathcal{H}_{1a}}$ and the 2-system of $\mathbf{J}_{\mathcal{H}_{1c}}$, as follows:

$$\mathbf{J}_{\mathcal{H}_1} = \begin{bmatrix} (\mathbf{c}_1^0 \times \mathbf{u}_1)^T & \mathbf{u}_1^T \\ (\mathbf{c}_2^0 \times \mathbf{u}_2)^T & \mathbf{u}_2^T \\ (\mathbf{c}_3^0 \times \mathbf{u}_3)^T & \mathbf{u}_3^T \\ (\mathbf{c}_4^0 \times \mathbf{u}_4)^T & \mathbf{u}_4^T \\ (\mathbf{m}_1 \times \mathbf{n}_1)^T & \mathbf{0}_{1\times3} \\ \mathbf{m}_2 \times \mathbf{n}_2)^T & \mathbf{0}_{1\times3} \end{bmatrix} \tag{15}$$

4.2   Operation Mode 2: Reversed Schönflies Mode ($\mathcal{H}_2$)

This operation mode is characterized by the second sub-ideal $\mathcal{H}_2$ in which parameters x_0 and x_3 are null. The parameters $x_0 = 0$ and $x_3 = 0$ are substituted into the transformation matrix, which gives:

$$\mathbf{T}_{\mathcal{H}_2} = \begin{pmatrix} x_1^2 - x_2^2 & 2x_1x_2 & 0 & X \\ 2x_1x_2 & -x_1^2 + x_2^2 & 0 & Y \\ 0 & 0 & -1 & Z \\ 0 & 0 & 0 & 1 \end{pmatrix} \tag{16}$$

The transformation matrix $\mathbf{T}_{\mathcal{H}_2}$ represents the 4-DOF motions performed by the moving-platform. This motion consists of 3-DOF translational motions parametrized by X, Y, Z and 1-DOF rotational motion parametrized by x_1 and x_2. The moving-platform was turned 180° from the identity condition about an axis parallel to the XY-plane. The identity condition is defined as a pose when the moving-frame and the fixed frame are coincident, i.e. $\Sigma_0 \equiv \Sigma_1$. As a consequence, the w-axis of the moving-frame Σ_1 is pointing downward. In this paper, this operation mode is called the reversed Schönflies mode. The screw systems of reversed Schönflies mode are the same as the Schönflies mode, i.e. Jacobian of constraint $\mathbf{J}_{\mathcal{H}_{2c}}$ and Jacobian of actuation $\mathbf{J}_{\mathcal{H}_{2a}}$, as defined in Eq. (13-14).

In practice, the reversed Schönflies mode is difficult to reach due to collisions within legs or collisions between leg and moving-platform. Thus, the following analysis will not include the reversed Schönflies mode.

4.3   Operation Mode 3: Additional Mode ($\mathcal{H}_3$)

This operation mode is characterized by the sub-ideal $\mathcal{H}_3$ which consists of nine polynomials. Its mathematical expressions are rather general and need further investigation. The last six polynomials are dependent to the first three polynomials. By solving the last six polynomials, it will lead to the first three. Thus, the three independent parameters X, x_3, x_2 are solved linearly in terms of the design parameters a, b, c, d from the first three polynomial sub-equations of the sub-ideal $\mathcal{H}_3$ in Eq. (11), as follows:

$$x_3 = \pm x_0 \sqrt{\frac{(c-a)(b-d)}{(a+c)(d+b)}}, \quad x_2 = \pm x_1 \sqrt{\frac{(c-a)(b+d)}{(b-d)(a+c)}}, \quad X = \pm Y \sqrt{\frac{d^2(c-a)(a+c)}{c^2(b-d)(d+b)}}. \tag{17}$$

Real solutions of Eq. (17) are obtained if one of these inequalities is satisfied, namely: $(c-a)(b-d) \geq 0$ or $\frac{(c-a)}{(b-d)} \geq 0$. Since both inequalities lead to the same results, only the first one is considered in this paper, namely $(c-a)(b-d) \geq 0$. Based on this inequality, four geometric constraints can be identified as follows:

1. Geometric constraint A: $c > a, b > d$ or $c < a, b < d$
2. Geometric constraint B: $c = a, b \neq d$
3. Geometric constraint C: $c \neq a, b = d$
4. Geometric constraint D: $c = a, b = d$

The geometric constraints A, B, C, and D determine the geometric relationships among the design parameters a, b, c, and d. By fulfilling these conditions, the 4-CRU parallel mechanism may generate Schönflies mode, reversed Schönflies mode, and new additional modes. To identify the additional modes, the primary decomposition must be recomputed, and the discussions are provided hereafter.

4.3.1 Geometric constraint A: $c > a, b > d$ or $c < a, b < d$

The additional mode of geometric constraint A is characterized by Eq. (17). One rotational motion is parametrized by parameters x_0, x_1 in connection with the normalization equation defined in Eq. (9). The absence of parameter Z indicates that the moving-platform is able to perform one translational motion along vertical direction and another translational motion defined by X related to Eq. (9). It shows that the 4-CRU parallel mechanism in this operation mode has 3-DOF motion. In this operation mode, the moving-platform is no longer parallel to the base and is tilted within $0°$ and $180°$.

By using the Screw theory, the Jacobian matrix of the additional mode can be determined. In this additional mode, the axis $\mathbf{n}_i$ is not pointing upward and is also not parallel to the axis $\mathbf{s}_i$, as shown in Fig. 6(b). In this configuration, the constraint screw reciprocal to five twists of CRU leg is a zero-pitch screw. This constraint screw passes through the intersection of axes $\mathbf{s}_i$ and $\mathbf{n}_i$ and is along the axis $\mathbf{s}_i \times \mathbf{n}_i$. The intersection point of the axes $\mathbf{s}_i$ and $\mathbf{n}_i$ is denoted by point Q_i and the constraint screw becomes: $\hat{\$}_{ci} = \begin{bmatrix} (\mathbf{s}_i \times \mathbf{n}_i) \\ \mathbf{q}_i^0 \times (\mathbf{s}_i \times \mathbf{n}_i) \end{bmatrix}$. Since vector $\mathbf{s}_i \times \mathbf{n}_i$ of four legs are geometrically parallel to each other as shown in Fig. 7, the constraint screws are 3-system. Three arbitrary constraint screws can be selected, e.g. $\hat{\$}_{c1}, \hat{\$}_{c2}, \hat{\$}_{c3}$ to form Jacobian of constraint, as:

$$\mathbf{J}_{\mathcal{H}_{3Ac}} = \begin{bmatrix} (\mathbf{q}_1^0 \times (\mathbf{s}_1 \times \mathbf{n}_1))^T & (\mathbf{s}_1 \times \mathbf{n}_1)^T \\ (\mathbf{q}_2^0 \times (\mathbf{s}_2 \times \mathbf{n}_2))^T & (\mathbf{s}_2 \times \mathbf{n}_2)^T \\ (\mathbf{q}_3^0 \times (\mathbf{s}_3 \times \mathbf{n}_3))^T & (\mathbf{s}_3 \times \mathbf{n}_3)^T \end{bmatrix} \tag{18}$$

With the moving-platform constraints described as a 3-system of screws, its motion is described by a reciprocal 3-system of twists, which is a planar 3-DOF motion in a plane perpendicular to the directions of these constraint screws.

By allowing the translational motion of the CRU leg be actuated, one actuation screw reciprocal to four passive joints can be identified. This actuation screw is collinear with vector $\mathbf{u}_i$ and passes through point B_i to C_i, as: $\hat{\$}_{ai} = \begin{bmatrix} \mathbf{u}_i \\ \mathbf{c}_i^0 \times \mathbf{u}_i \end{bmatrix}$. The number of actuation screws required in this operation mode are redundant and the actuation screws are 3-system. Three arbitrary actuation screws, e.g. $\hat{\$}_{a1}, \hat{\$}_{a2}, \hat{\$}_{a3}$ can be selected to form the Jacobian of actuation, as follows:

$$\mathbf{J}_{\mathcal{H}_{3Aa}} = \begin{bmatrix} (\mathbf{c}_1^0 \times \mathbf{u}_1)^T & \mathbf{u}_1^T \\ (\mathbf{c}_2^0 \times \mathbf{u}_2)^T & \mathbf{u}_2^T \\ (\mathbf{c}_3^0 \times \mathbf{u}_3)^T & \mathbf{u}_3^T \end{bmatrix} \tag{19}$$

Eventually, the Jacobian matrix $\mathbf{J}_{\mathcal{H}_{3A}}$ consists of 3-system actuation screws and 3-system constraint screws, as follows:

$$\mathbf{J}_{\mathcal{H}_{3A}} = \begin{bmatrix} (\mathbf{c}_1^0 \times \mathbf{u}_1)^T & \mathbf{u}_1^T \\ (\mathbf{c}_2^0 \times \mathbf{u}_2)^T & \mathbf{u}_2^T \\ (\mathbf{c}_3^0 \times \mathbf{u}_3)^T & \mathbf{u}_3^T \\ (\mathbf{q}_1^0 \times (\mathbf{s}_1 \times \mathbf{n}_1))^T & (\mathbf{s}_1 \times \mathbf{n}_1)^T \\ (\mathbf{q}_2^0 \times (\mathbf{s}_2 \times \mathbf{n}_2))^T & (\mathbf{s}_2 \times \mathbf{n}_2)^T \\ (\mathbf{q}_3^0 \times (\mathbf{s}_3 \times \mathbf{n}_3))^T & (\mathbf{s}_3 \times \mathbf{n}_3)^T \end{bmatrix} \tag{20}$$

4.3.2 Geometric Constraint B: $c = a$ and $b \neq d$

Let us consider the design parameters where the base and moving-platform follow the geometric constraint B, i.e. $c = a$ and $b \neq d$. This condition is then substituted into the constraint equations f_1, f_2, f_3, f_4 defined in Eq. (7). The
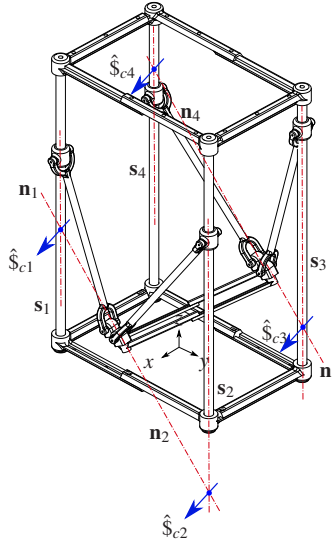
Fig. 7: Additional mode of geometric constraint A

new polynomial ideal $\mathcal{H}_B$ is defined and the primary decomposition is computed. The ideal $\mathcal{H}_B$ is decomposed into three components, $\mathcal{H}_B = \bigcap_{j=1}^{3} \mathcal{H}_{jB}$, with the results of primary decomposition as follows:

$$
\begin{aligned}
\mathcal{H}_{1B} &: \langle x_1, x_2 \rangle \\
\mathcal{H}_{2B} &: \langle x_0, x_3 \rangle \\
\mathcal{H}_{3B} &: \langle X, x_2, x_3 \rangle
\end{aligned}
\tag{21}
$$

The results of primary decomposition tells us that the 4-CRU parallel mechanism with the geometric constraint A has three operation modes. The first and second sub-ideals $\mathcal{H}_{1B}$ and $\mathcal{H}_{2B}$ correspond to the Schönflies and reversed Schönflies modes, hence $\mathcal{H}_{1B} = \mathcal{H}_1$ and $\mathcal{H}_{2B} = \mathcal{H}_2$. The third sub-ideal $\mathcal{H}_{3B}$ is associated with a specific operation mode. The Hilbert dimension is computed as: $\dim(\mathcal{H}_{3B}) = 3$. This shows that the sub-ideal $\mathcal{H}_{3B}$ is 3-DOF operation mode. The third operation mode is characterized by the parameters $X = 0, x_2 = 0, x_3 = 0$, which are substituted into the transformation matrix as follows:

$$
\mathbf{T}_{\mathcal{H}_{3B}} = \begin{pmatrix}
1 & 0 & 0 & 0 \\
0 & x_0^2 - x_1^2 & -2x_0 x_1 & Y \\
0 & 2x_0 x_1 & x_0^2 - x_1^2 & Z \\
0 & 0 & 0 & 1
\end{pmatrix}
\tag{22}
$$

The transformation matrix $\mathbf{T}_{\mathcal{H}_{3B}}$ shows that the motion type belonging to the third mode is composed of 2-DOF translational motions parametrized by Y and Z and 1-DOF rotational motion parametrized by x_0 and x_1. This motion type is also well-known as a planar motion with pure rotational motion about x-axis. One pose of the mechanism in this additional mode $\mathcal{H}_{3B}$ is shown in Fig. 8.

4.3.3 Geometric Constraint C: $c \neq a$ and $b = d$

According to geometric constraint C, the design parameters of the base and moving-platform satisfy $c \neq a$ and $b = d$. The new constraint equations are derived by substituting $c \neq a$ and $b = d$ into Eq. (7). These new constraint equations are then collected to be a polynomial ideal $\mathcal{H}_C$. The primary decomposition is computed over the ideal $\mathcal{H}_C$. Similar to the ideal $\mathcal{H}_B$, the ideal $\mathcal{H}_C$ is also decomposed into three sub-ideals, as: $\mathcal{H}_C = \bigcap_{j=1}^{3} \mathcal{H}_{jC}$ with their results as follows:

$$
\begin{aligned}
\mathcal{H}_{1C} &: \langle x_1, x_2 \rangle \\
\mathcal{H}_{2C} &: \langle x_0, x_3 \rangle \\
\mathcal{H}_{3C} &: \langle Y, x_1, x_3 \rangle
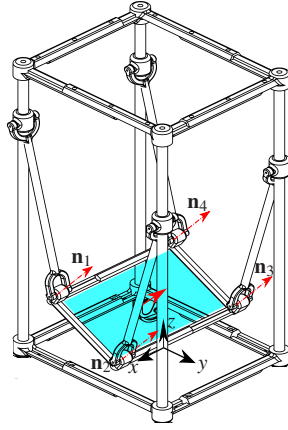\end{aligned}
\tag{23}
$$

Fig. 8: Additional mode of geometric constraint B

The first and second sub-ideals $\mathcal{H}_{1C}$ and $\mathcal{H}_{2C}$ correspond to the Schönflies and reversed Schönflies modes, hence $\mathcal{H}_{1C} = \mathcal{H}_1$ and $\mathcal{H}_{2C} = \mathcal{H}_2$. The third sub-ideal is a 3-DOF operation mode which is shown by the computation of the Hilbert dimension as: $\dim(\mathcal{H}_{3C}) = 3$. Unlike the geometric constraint B, the planar motion of the third mode $\mathcal{H}_{3C}$ is composed of 2-DOF translational motions about xy-plane and 1-DOF rotational motion about y-axis. This planar motion is characterized by $Y = 0, x_1 = 0, x_3 = 0$ which are substituted into the transformation matrix as given in Eq. (24). The illustration of mechanism pose in this additional mode $\mathcal{H}_{3C}$ is shown in Fig. 9.

$$\mathbf{T}_{\mathcal{H}_{3C}} = \begin{pmatrix} x_0^2 - x_2^2 & 0 & 2x_0x_2 & X \\ 0 & 1 & 0 & 0 \\ -2x_0x_2 & 0 & x_0^2 - x_2^2 & Z \\ 0 & 0 & 0 & 1 \end{pmatrix} \tag{24}$$
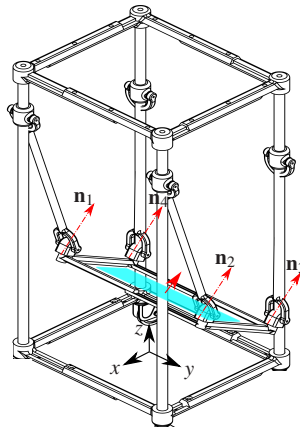
Fig. 9: Additional mode of geometric constraint C

4.3.4 Geometric Constraint D: $c = a$ and $b = d$

In the geometric constraint D, the design parameters of the base and moving-platform are assigned to be $c = a$ and $b = d$. This condition is substituted into the constraint equations f_1, f_2, f_3, f_4 derived in Eq. (7). The polynomial ideal $\mathcal{H}_D$ is defined by collecting the new constraint equations. Like the two ideals $\mathcal{H}_B$ and $\mathcal{H}_C$, the computation of primary decomposition shows

that the ideal $\mathcal{H}_D$ is decomposed into three sub-ideals, as: $\mathcal{H}_D = \bigcap_{j=1}^{3} \mathcal{H}_{jC}$. The results are:

$$
\begin{aligned}
\mathcal{H}_{1D} &: \langle x_1, x_2 \rangle \\
\mathcal{H}_{2D} &: \langle x_0, x_3 \rangle \\
\mathcal{H}_{3D} &: \langle X x_1 + Y x_2, x_3 \rangle
\end{aligned}
\tag{25}
$$

The first and second sub-ideals $\mathcal{H}_{1D}$ and $\mathcal{H}_{2D}$ are associated with the Schönflies and reversed Schönflie modes, hence $\mathcal{H}_{1D} = \mathcal{H}_1$ and $\mathcal{H}_{2D} = \mathcal{H}_2$. Unlike the third operation modes of geometric constraints B and C, this third operation mode has 4-DOF motions, which is shown by the computation of the Hilbert dimension, i.e. $\dim(\mathcal{H}_{3D}) = 4$. Based on Eq. (25), the parameter X can be solved linearly from the sub-ideal $\mathcal{H}_{3D}$ as: $X = -\dfrac{Y x_2}{x_1}$. It shows that the moving-platform will undergo parasitic translation motion. To determine the motion type of this mode, the parameters $X = -\dfrac{Y x_2}{x_1}$ and $x_3 = 0$ are substituted into the transformation matrix, as follows:

$$
\mathbf{T}_{\mathcal{H}_{3D}} =
\begin{pmatrix}
x_0^2 + x_1^2 - x_2^2 & 2x_1 x_2 & 2x_0 x_2 & -\dfrac{Y x_2}{x_1} \\
2x_1 x_2 & x_0^2 - x_1^2 + x_2^2 & -2x_0 x_1 & Y \\
-2x_0 x_2 & 2x_0 x_1 & x_0^2 - x_1^2 - x_2^2 & Z \\
0 & 0 & 0 & 1
\end{pmatrix}
\tag{26}
$$

Accordingly, the moving-platform can perform 2-DOF translational motion which are parametrized by Y and Z and 2-DOF rotational motions which are parametrized by x_0, x_1, x_2 in connection with the normalization equation. The 2-DOF rotational motions are about x-axis and y-axis. The pose of 4-CRU parallel mechanism in the additional mode $\mathcal{H}_{3D}$ is depicted in Fig. 10.
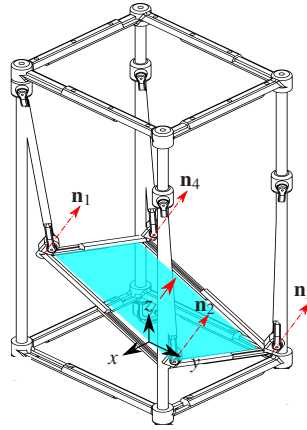
Fig. 10: Additional mode of geometric constraint D

5   Workspace and Actuation Singularities for Different Operation Modes
5.1   Workspace

The workspace of a 4-CRU parallel mechanism will be analyzed for different operation modes. The workspace will be defined as a set of positions that can be reached by an arbitrary specified point in the moving-platform for a given orientation. Without loss of generality, the middle point of the moving-platform was selected to illustrate the workspace. The limit of passive joints and link collisions are negligible. The limit of active joints is assumed to be equal to the frame height, i.e. $h_{i_{min}} = 0$ and $h_{i_{max}} = 4$. Therefore, the workspace boundary will be determined by the dimensions of design parameters and the limit of active joints.

Let us consider geometric constraint A, i.e. $a = \frac{7}{4}, b = 2, c = 2, d = 1, r = \frac{5}{2}$ in the Scönflies mode. The moving-platform is assumed to be working at a specific orientation, namely $x_0 = 1, x_1 = x_2 = x_3 = 0$. A set of constraint equations f_5, f_6, f_7, f_8 is recalled as follows:

$$
\begin{aligned}
f_5 &: 16X^2 + 16Y^2 + 16Z^2 + 8X + 32Y - 96Z + 61 = 0 \\
f_6 &: 16X^2 + 16Y^2 + 16Z^2 + 8X - 32Y - 96Z + 61 = 0 \\
f_7 &: 16X^2 + 16Y^2 + 16Z^2 - 8X - 32Y - 96Z + 61 = 0 \\
f_8 &: 16X^2 + 16Y^2 + 16Z^2 - 8X + 32Y - 96Z + 61 = 0
\end{aligned}
\tag{27}
$$

Equation (27) represents tubular regions of four legs as shown in Fig. 11(a) and its cross-section is shown in Fig. 11(b). The intersection of the four tubular regions (pink color) yields the workspace (blue color) as shown in Fig. 11(b). The same approach was carried out to determine the workspace of Schönflies mode and additional mode for geometric constraint A, B, C, D as shown in Table 1. The blue and yellow surfaces in Table 1 depict the workspace of Schönflies modes and an additional mode, respectively. Their projections in 2-dimensional space are also given in Table 1.

| (a) Isometric view | (b) Top view |
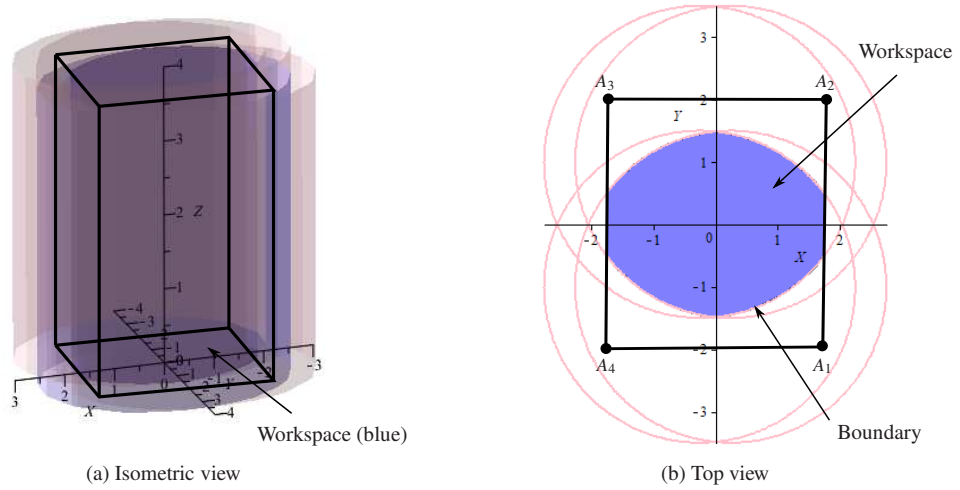
Fig. 11: Cartesian workspace for orientation $x_0 = 1, x_1 = x_2 = x_3 = 0$
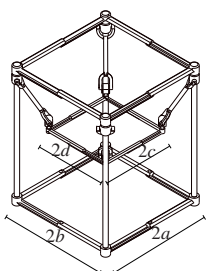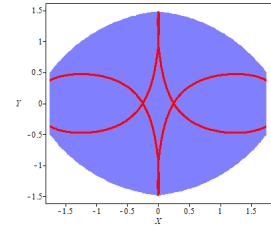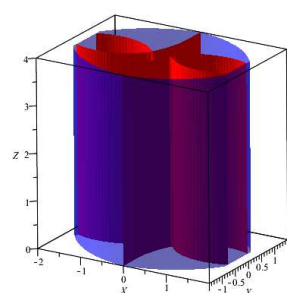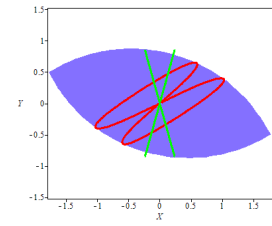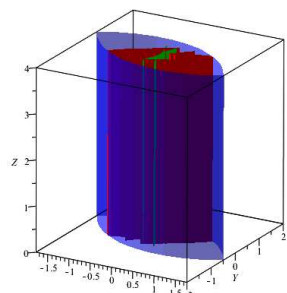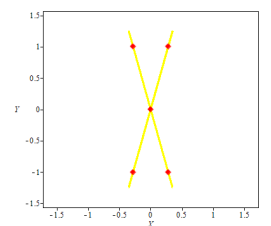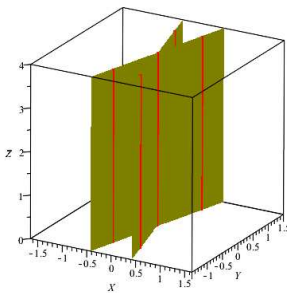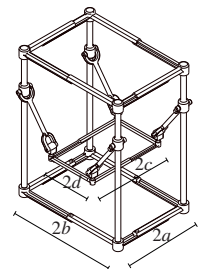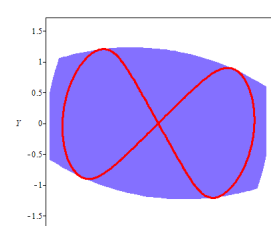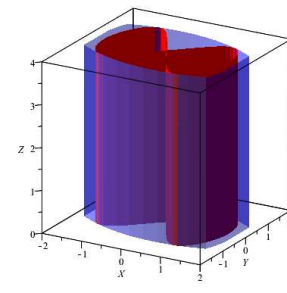
5.2 Actuation Singularities

The singular configurations are those where the actuators cannot control the velocity of moving-platform hence it loses the ability to transmit motion and forces, is called *actuation singularity* in [25]. It typically occurs inside an operation mode. The 4-CRU parallel mechanism reaches an actuation singularity when the determinant of Jacobian matrix of each operation mode vanishes. Initially, an ideal that consists of inverse kinematic equations is defined as follows:

$$
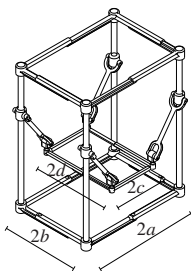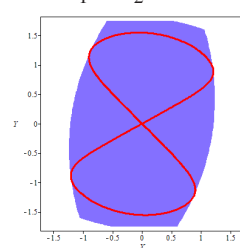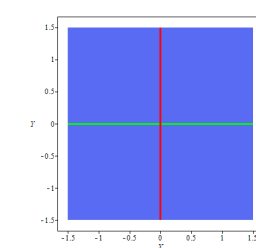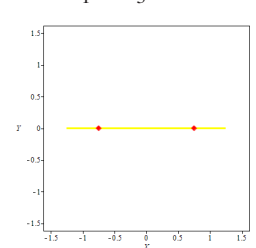\mathcal{K} = \langle f_5, f_6, f_7, f_8, f_9 \rangle
\tag{28}
$$
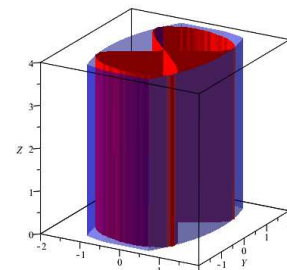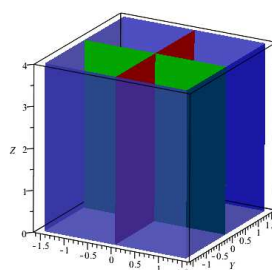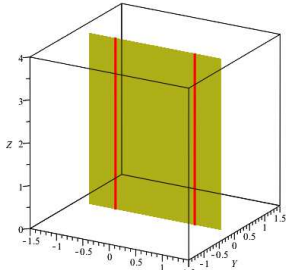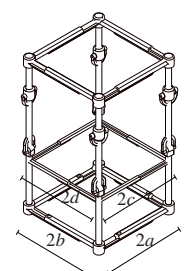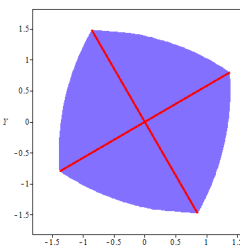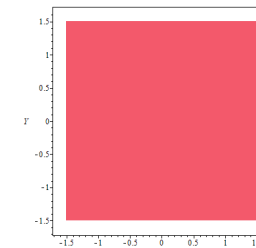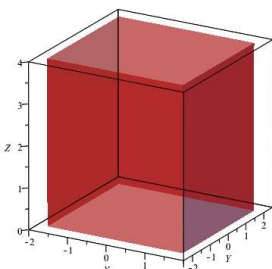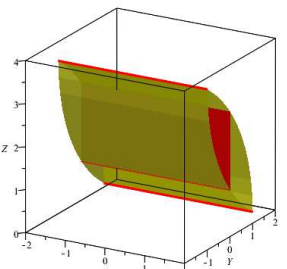
Hence, an ideal of each operation mode can be defined by the linear combination of $\mathcal{H}$ and $\mathcal{K}$, such that: $\mathcal{L} = \mathcal{H} \cup \mathcal{K}$. The Jacobian matrix is determined by taking first-order partial derivative of system $\mathcal{L}$ with respect to the corresponding motion

Table 1: Workspace and singularities of different operation modes

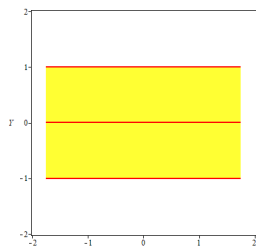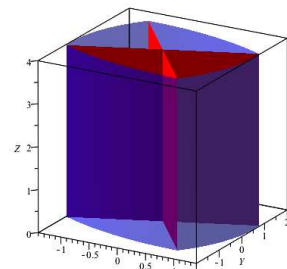| Geometric constraint	Design parameters	Workspace		
		Schönflies mode	Transition	Additional mode
A		$x_0 = 1, x_1 = x_2 = x_3 = 0$	$x_0 = -\frac{\sqrt{230}}{46}, x_3 = -\frac{\sqrt{46}}{46}$ $x_1 = x_2 = 0$	$x_1 = \frac{\sqrt{15}}{6}, x_2 = \frac{\sqrt{3}}{6}$ $x_0 = \frac{3\sqrt{115}}{46}, x_3 = \frac{\sqrt{23}}{46}$
	$a = \frac{7}{4}$ $b = 2$ $c = 2$ $d = 1$ $r = \frac{5}{2}$			
B		$x_0 = \frac{\sqrt{3}}{2}, x_3 = \frac{1}{2}$ $x_1 = x_2 = 0$	$x_0 = 1, x_1 = x_2 = x_3 = 0$	$x_0 = \frac{\sqrt{3}}{2}, x_1 = \frac{1}{2}$ $x_2 = x_3 = 0$
	$a = \frac{7}{4}$ $b = 2$ $c = \frac{7}{4}$ $d = \frac{3}{2}$ $r = 4$			

Legend: ● = Schönflies mode workspace, ● = additional mode workspace   , ● = actuation singularity, ● = constraint singularity

Table 1: Continued

Geometric constraint	Design parameters	Workspace		
		Schönflies mode	Transition	Additional mode
C		$x_0 = \frac{\sqrt{3}}{2}, x_3 = \frac{1}{2}$ $x_1 = x_2 = 0$	$x_0 = 1, x_1 = x_2 = x_3 = 0$	$x_0 = \frac{\sqrt{3}}{2}, x_2 = \frac{1}{2}$ $x_1 = x_3 = 0$
	$a = 2$ $b = \frac{7}{4}$ $c = \frac{3}{2}$ $d = \frac{7}{4}$ $r = 4$			
D		$x_0 = \frac{\sqrt{3}}{2}, x_3 = \frac{1}{2}$ $x_1 = x_2 = 0$	$x_0 = 1, x_1 = x_2 = x_3 = 0$	$x_0 = \frac{1}{2}, x_1 = -\frac{\sqrt{3}}{2}$ $x_2 = x_3 = 0$
	$a = \frac{7}{4}$ $b = 2$ $c = \frac{7}{4}$ $d = 2$ $r = 4$			

Legend: ● = Schönflies mode workspace, ● = additional mode workspace , ● = actuation singularity, ● = constraint singularity

parameters, as follows:

$$
\begin{aligned}
\text{Schönflies mode} &&& \mathbf{J}_1 = \frac{\partial \mathcal{L}_1}{\partial(x_0, x_3, X, Y, Z)} = \frac{\partial(\mathcal{H}_1 \cup \mathcal{K})}{\partial(x_0, x_3, X, Y, Z)}\\[2mm]
\text{Reversed Schönflies mode} &&& \mathbf{J}_2 = \frac{\partial \mathcal{L}_2}{\partial(x_1, x_2, X, Y, Z)} = \frac{\partial(\mathcal{H}_2 \cup \mathcal{K})}{\partial(x_1, x_2, X, Y, Z)}\\[2mm]
\text{Additional mode (A)} &&& \mathbf{J}_{3A} = \frac{\partial \mathcal{L}_{3A}}{\partial(x_2, x_3, Y, Z)} = \frac{\partial(\mathcal{H}_{3A} \cup \mathcal{K})}{\partial(x_2, x_3, Y, Z)}\\[2mm]
\text{Additional mode (B)} &&& \mathbf{J}_{3B} = \frac{\partial \mathcal{L}_{3B}}{\partial(x_0, x_1, Y, Z)} = \frac{\partial(\mathcal{H}_{3B} \cup \mathcal{K})}{\partial(x_0, x_1, Y, Z)}\\[2mm]
\text{Additional mode (C)} &&& \mathbf{J}_{3C} = \frac{\partial \mathcal{L}_{3C}}{\partial(x_0, x_2, X, Z)} = \frac{\partial(\mathcal{H}_{3C} \cup \mathcal{K})}{\partial(x_0, x_2, X, Z)}\\[2mm]
\text{Additional mode (D)} &&& \mathbf{J}_{3D} = \frac{\partial \mathcal{L}_{3D}}{\partial(x_0, x_1, x_2, Y, Z)} = \frac{\partial(\mathcal{H}_{3D} \cup \mathcal{K})}{\partial(x_0, x_1, x_2, Y, Z)}
\end{aligned}
\tag{29}
$$

The determinant is computed for all Jacobian matrices in Eq. (29). Each determinant of the Jacobian matrices is added into the corresponding system $\mathcal{L}$ and the actuated lengths (h_1, h_2, h_3, h_4) are eliminated. It yields a single equation in terms of rotations and translations which is known as an equation of actuation singularity. This equation defines an actuation singularity surface which is illustrated within the mechanism workspace in red surface as given in Table 1. Their projection in 2-dimensional space is also plotted within the mechanism workspace as shown in Table 1. The actuation singularity and mechanism workspace are depicted when the moving-platform is in the Schönflies mode, transition region and additional mode for four types of geometric constraints.

6   Reconfiguration Between Operation Modes

Reconfiguration has been studied by many researchers since it is an important issue in control of parallel mechanisms with multiple operation modes. The 4-CRU parallel mechanism can reconfigure itself from one operation mode to another by passing through the transition configurations. The transition configurations based on [12, 13] are defined as common configurations that belong to more than one operation mode, and are also known as constraint singularity configurations. To determine the transition configurations, the linear combination of two polynomial ideals was performed. All reconfiguration conditions between each pair of different operation modes are identified and provided in Table 2.

Let the 4-CRU parallel mechanism have geometric constraint B, i.e. $a = c, b \neq d$. The design parameters are assigned to be $a = c = \frac{7}{4}, b = 2, d = \frac{3}{2}$. Initially, the moving-platform is in the Schönflies mode $\mathcal{H}_1$. It will switch to the additional mode $\mathcal{H}_{3B}$ by entering the transition configurations which can be determined by the linear combination of those two polynomial ideals as follows: $\mathcal{H}_1 \cup \mathcal{H}_{3B} = \langle x_1, x_2, x_3, X \rangle$. The moving-platform is said to be at the transition configurations whenever its orientation is similar to the base and its geometric center P is on the plane $X = 0$. The transition region is plotted within the mechanism workspace in green surface as given in Table 1.

Once the moving-platform leaves the transition configurations, the moving-platform will switch to the additional mode $\mathcal{H}_{3B}$. As explained in Section 4.3, the moving-platform in the additional mode $\mathcal{H}_{3B}$ is able to perform 3-DOF planar motion on the plane $X = 0$. The moving-platform is no longer parallel to the base and its orientation is defined by x_0, x_1 in connection with the normalization equation. The reconfiguration is demonstrated by the mock-up as shown in Fig. 12 and its animation is provided here[2].

7   Self-motions in Schönflies Mode

In this section, the conditions of the actuated leg lengths $h_i, i = 1..4$ are derived such that the mechanism can exhibit at least 1-DOF self-motion in the Schönflies mode. In Schönflies mode, the moving-platform performs only 1-DOF rotation about z-axis characterized by two parameters x_0, x_3. These parameters are replaced by the tangent of the half-angle hence

---

[2]http://its.id/4crumanipulator

Table 2: Reconfiguration conditions

Geometric constraint	Mode reconfiguration	Transition region
A	$\mathcal{H}_1 \cup \mathcal{H}_{3A}$	$x_1 = 0; \ x_2 = 0;$
		$c^2(b-d)(d+b)X^2 + d^2(a-c)(a+c)Y^2 = 0;$
		$(a+c)(d+b)x_3^2 - (c-a)(b-d)x_0^2 = 0.$
B	$\mathcal{H}_1 \cup \mathcal{H}_{3B}$	$x_0 = 1; \ x_1 = 0; \ x_2 = 0; \ x_3 = 0; \ X = 0$
C	$\mathcal{H}_1 \cup \mathcal{H}_{3C}$	$x_0 = 1; \ x_1 = 0; \ x_2 = 0; \ x_3 = 0; \ Y = 0$
D	$\mathcal{H}_1 \cup \mathcal{H}_{3D}$	$x_0 = 1, x_1 = 0; \ x_2 = 0; \ x_3 = 0$

(a) Schönflies mode   (b) Transition   (c) Additional mode
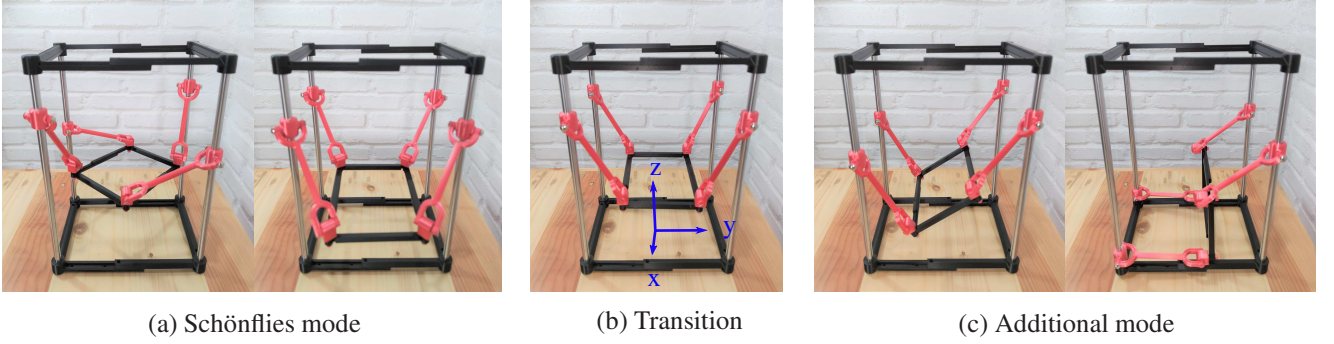
Fig. 12: Reconfiguration of Geometric constraint B

1-DOF rotation can be represented by a single parameter t_p, as follows:

$$x_0 = \frac{1 - t_p^2}{1 + t_p^2}, \qquad x_3 = \frac{2t_p}{1 + t_p^2} \qquad (30)$$

This paremetrization is substituted into the ideal $\mathcal{L}_1 = \mathcal{H}_1 \cup \mathcal{K}$. Then one can compute an elimination of parameters X, Y, Z and it yields a univariate polynomial of degree 16 in one parameter t_p, as follows:

$$G_0 : \delta_{16}t_p^{16} + \delta_{15}t_p^{15} + \delta_{14}t_p^{14} + \delta_{13}t_p^{13} + \delta_{12}t_p^{12} + \delta_{11}t_p^{11} + \delta_{10}t_p^{10} + \delta_9 t_p^9 + \delta_8 t_p^8 + \delta_7 t_p^7 + \delta_6 t_p^6 + \delta_5 t_p^5 + \delta_4 t_p^4 + \delta_3 t_p^3 + \delta_2 t_p^2 +$$
$$\delta_1 t_p + \delta_0 = 0$$

$$(31)$$

where coefficients $\delta_0 ... \delta_{16}$ are polynomials in terms of the actuated leg lengths h_1, h_2, h_3, h_4 and the design parameters a, b, c, d, r. The self-motions occur if all coefficients simultaneously vanish. The coefficient δ_0 is the absolute term in G_0 as:

$$\delta_0 : 16(b-d)^2(a-c)^2(a^2 - 2ac + b^2 - 2bd + c^2 + d^2 - r^2)\gamma_1^2 + (a-c)^2\gamma_2^2\gamma_3^2\gamma_4^2 + (b-d)^2\gamma_5^2\gamma_6^2\gamma_7^2 + 4(b-d)^2(a-c)^2\gamma_8\gamma_9 \quad (32)$$

where:

$$\gamma_1 : h_1 - h_2 + h_3 - h_4 \qquad \gamma_2 : -h_4 + h_1 - h_3 + h_2 \qquad \gamma_3 : h_1 - h_2$$
$$\gamma_4 : h_3 - h_4 \qquad \gamma_5 : h_4 + h_1 - h_3 - h_2 \qquad \gamma_6 : h_1 - h_4 \qquad (33)$$
$$\gamma_7 : -h_3 + h_2 \qquad \gamma_8 : h_1^2 - 2h_1h_2 + h_2^2 + h_3^2 - 2h_3h_4 + h_4^2 \qquad \gamma_9 : h_1^2 - 2h_1h_4 + h_2^2 - 2h_2h_3 + h_3^2 + h_4^2$$

Let the coefficient δ_0 vanish due to the conditions of the actuated leg lengths. The conditions of the actuated leg lengths for which $\delta_0 = 0$ can be obtained by solving γ_1 to γ_9 in Eq. (33). This computation leads to two conditions of the actuated leg lengths, as follows:

$$
\begin{aligned}
&\text{Condition 1}: \quad h_1 = h_2 = h_3 = h_4 \\
&\text{Condition 2}: \quad h_1 = h_2, h_3 = h_4 \ \ \text{or} \ \ h_1 = h_4, h_2 = h_3
\end{aligned}
\tag{34}
$$

Each of these two conditions is substituted back into the univariate polynomial G_0. It turns out that both substitutions give the same factor $(ad - bc)$, as follows:

$$
\begin{aligned}
&\text{From Condition 1} \quad G_0 : (ad - bc)\left(\kappa_0 t_p^4 + \kappa_1 t_p^2 + \kappa_2\right) = 0 \\
&\text{From Condition 2} \quad G_0 : (ad - bc)\left(\kappa_3 t_p^8 + \kappa_4 t_p^6 + \kappa_5 t_p^4 + \kappa_6 t_p^2 + \kappa_7\right) = 0
\end{aligned}
\tag{35}
$$

where $\kappa_0 ... \kappa_7$ are the coefficients in terms of only design parameters a, b, c, d, r. If the first factor $(ad - bc)$ vanishes, one can obtain the self-motions. To illustrate the self-motions, certain values are assigned to the design parameters and actuated leg lengths in the following.

7.1 Condition 1: $h_1 = h_2 = h_3 = h_4$

Let the base and moving-platform be the same shape but not the same dimension. A square shape is considered such that it fulfils $(ad - bc) = 0$. The design parameters are assigned to be: $a = b = 2$, $c = d = 1$, $r = 3$. In condition 1, all four actuated leg lengths are equal such that: $h_1 = h_2 = h_3 = h_4 = 1$. By substituting all those values into the ideal $\mathcal{L}_1$, the solutions of direct kinematics can be computed and the parameters X, Y, Z, x_0, x_3 can be solved. It appears that the parameter Z is free such that the transformation matrix becomes:

$$
\mathbf{T} = \begin{pmatrix}
1 & 0 & 0 & 0 \\
0 & \dfrac{Z^2}{8} - \dfrac{Z}{4} + \dfrac{1}{4} & -\dfrac{1}{8}\sqrt{Z^2 - 2Z + 10}\sqrt{-Z^2 + 2Z + 6} & 0 \\
0 & \dfrac{1}{8}\sqrt{Z^2 - 2Z + 10}\sqrt{-Z^2 + 2Z + 6} & \dfrac{Z^2}{8} - \dfrac{Z}{4} + \dfrac{1}{4} & 0 \\
Z & 0 & 0 & 1
\end{pmatrix}
\tag{36}
$$

The transformation matrix shown in Eq. (36) parametrizes 1-DOF self-motion which can be performed by the moving-platform. The platform is able to simultaneously rotate and translate about the z-axis. Although all four actuated leg lengths are fixed with the same values, the moving-platform is able to move as demonstrated by the mock-up in Fig. 13 and its animation is provided here[3].

Fig. 13: Self-motion of Condition 1

---

[3]http://its.id/4crumanipulator

7.2 Condition 2: $h_1 = h_4, h_2 = h_3$ **or** $h_1 = h_2, h_3 = h_4$

There are two possibilities of condition 2, namely $h_1 = h_4, h_2 = h_3$ or $h_1 = h_2, h_3 = h_4$. In fact, these possibilities are swapped by the x and y axes. The following analysis will discuss only one, namely $h_1 = h_2, h_3 = h_4$.

The geometric constraint D ($c = a, b = d$) is selected such that it fulfills $(ad - bc) = 0$. The geometric constraint D shows that the base and moving-platform are the same size and shape. Specific values are assigned to the design parameters as: $a = c = 1, b = d = 2, r = 3$. Likewise, the actuated leg lengths are assigned with certain values to fulfil condition 2 as: $h_1 = h_2 = 4, h_3 = h_4 = 1$. All these values are substituted into the ideal $\mathcal{L}_1$ and one can compute the solutions of direct kinematics by solving the parameters X, Y, Z, x_0, x_3. It turns out that the parameter X is free and the transformation matrix becomes:

$$\mathbf{T} = \begin{pmatrix} 1 & 0\ 0\ 0 \\ X & 1\ 0\ 0 \\ -\dfrac{\sqrt{-4X^2 + 27}}{5^2} & 0\ 1\ 0 \\ \dfrac{5}{2} & 0\ 0\ 1 \end{pmatrix} \tag{37}$$

The transformation matrix given in Eq. (37) shows that the moving-platform has 1-DOF self-motion while all actuated leg lengths are fixed. The platform is able to perform circular-translation in the xy-plane without change in orientation. Fig. 14 illustrates the 4-CRU parallel mechanism in one pose of self-motion and the trajectory followed by the moving-platform during the self-motion.
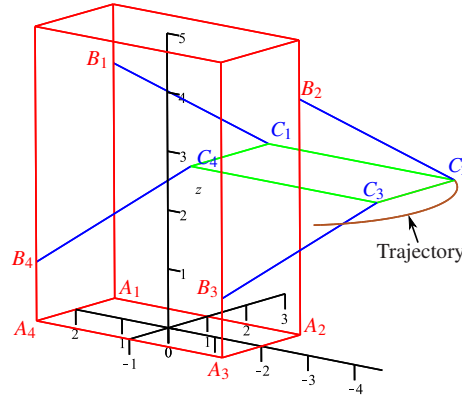

Fig. 14: Self-motion of Condition 2

8 Conclusions

Many printing mechanisms moves in 3-DOF translational motions, hence printability is degraded when they should print complex shapes and/or overhang geometry. This paper proposed a 4-CRU parallel mechanism to address those problems since this mechanism is able to change its operation modes through a series of reconfiguration process. This paper focused on the reconfiguration analysis and self-motions of a 4-CRU parallel mechanism based on their geometric constraints. The algebraic geometry approach was employed to define the constraint equations. The primary decomposition was computed over a set of constraint equations to determine four geometric constraints and each has three operation modes. The three operation modes are the Schönflies mode, the reversed Schönflies mode, and the additional mode which can be either 4-DOF or 3-DOF modes. Among these operation modes, the workspace and singularities were examined. The regions in which the reconfiguration takes place were obtained and geometrically plotted. Two conditions of the actuated leg lengths at which the moving-platform can perform at least 1-DOF self-motions in the Schönflies mode were detected and demonstrated in video. Deeper evaluation on the reconfiguration strategy and algorithm involving dynamic analysis, will be the subject of our future work. The future work fully rely upon the results reported in this paper.

Acknowledgement

References

[1] K. Wohlhart, "Kinematotropic Linkages", In: Lenarcic J. Parenti-Castelli V., Advances in Robot Kinematics, Kluwer, Dordrecht, pp. 359–368, 1996.

[2] X. Kong, "A Variable-DOF Single-loop 7R Spatial Mechanism with Five Motion Modes", Mechanism and Machine Theory, **120**, pp. 239–249, 2018.

[3] D. M. Gan, J. S. Dai, J. Dias, L. D. Seneviratne, "Variable Motion/Force Transmissibility of a Metamorphic Parallel Mechanism with Reconfigurable 3T and 3R Motion", ASME Journal of Mechanisms and Robotics, **8**(5), pp. 051001-1–051001-9, 2016.

[4] D. M. Gan, J. Dias, L. Seneviratne, "Unified Kinematics and Optimal Design of a 3-rRPS Metamorphic Parallel Mechanism with Reconfigurable Joint", Mechanism and Machine Theory, **96**, pp. 239–254, 2016.

[5] K. Xu, L. Li, S. Bai, Q. Yang, X. Ding, "Design and Analysis of a Metamorphic Mechanism Cell for Multistage Orderly Deployable/retractable Mechanism", Mechanism and Machine Theory, **111**, pp. 85-98, 2017.

[6] H. Xiu, K. Wang, T. Xu, G. Wei, L. Ren, "Archimedean Mechanisms Based on a Overconstrained Eight-bar Linkage", Mechanism and Machine Theory, **137**, pp. 476–508, 2019.

[7] G. Wei, Y. Chen, J. S. Dai, "Synthesis, Mobility, and Multifurcation of Deployable Polyhedral Mechanisms with Radially Reciprocating Motion", ASME Journal of Mechanical Design, **146**, pp. 091003-1–12, 2014.

[8] G. Wei, J. S. Dai, "A Spatial Eight-Bar Linkage and Its Association with the Deployable Platonic Mechanisms", ASME Journal of Mechanisms and Robotics, **6**, pp. 021010-1–9, 2014.

[9] L. Carbonari, M. Callegari, G. Palmieri, M.-C. Palpacelli, "A New Class of Reconfigurable Parallel kinematic Machines", Mechanism and Machine Theory, **79**, pp. 173-183, 2014.

[10] R. Rodriguez-Castro. "A New Parallel Manipulator with Multiple Operation Modes", Jounal of Mechanism and Robotics, **10**, pp. 1–9, 2018.

[11] D. Zlatanov, I. Bonev, C. Gosselin. "Constraint Singularities as C-space Singularities", In: J. Lenarcic and F. Thomas, Advances in Robot Kinematics, Theory and Applications, pp. 183–192, 2002.

[12] X. Kong. "Reconfiguration Analysis of a 4-DOF 3-RER Parallel Manipulator with Equilateral Triangular Base and moving-platform", Mechanism and Machine Theory, **98**, pp. 180–189, 2016.

[13] X. Kong. "Reconfiguration Analysis of a 3-DOF Parallel Mechanism Using Euler Parameter Quaternions and Algebraic Geometry Method", Mechanism and Machine Theory, **74**, pp. 188–201, 2014.

[14] L. Nurahmi, S. Caro, P. Wenger, J. Schadlbauer, M. Husty, "Reconfiguration Analysis of A 4-RUU Parallel Manipulator", Mechanism and Machine Theory, **96**, pp. 269–289, 2016.

[15] L. Nurahmi, S. Caro, P. Wenger, "Operation modes and self-motions of a 2-RUU parallel manipulator", Mechanism and Machine Science, **33**, pp. 417–426, 2015.

[16] L. Nurahmi, D. Gan, "Reconfiguration of a 3-(rR)PS Metamorphic Parallel Mechanism Based on Complete Workspace and Operation Mode Analysis", Journal of Mechanisms and Robotics, **12**, pp. 011002-1–15, 2020.

[17] L. Nurahmi, M. Husty, D. Gan, "Forward Kinematics and Singularities of a 3-(rR)PS Metamorphic Parallel Mechanism", USCToMM Symposium on Mechanical Systems and Robotics, pp. 68-77, 2020.

[18] L. Nurahmi, S. Caro, M. Solichin, "A novel ankle rehabilitation device based on a reconfigurable 3-RPS parallel manipulator", Mechanism and Machine Theory, **134**, pp. 135–150, 2019.

[19] H. Zhang, S. K. Agrawal. "Kinematic Design of a Dynamic Brace for Measurement of Head/Neck Motion", IEEE Robotics and Automation Letters, **2**(3), pp. 1428–1435, 2017.

[20] H. Zhang, K. Albee, S. K. Agrawal. "A spring-loaded compliant neck brace with adjustable supports", Mechanism and Machine Theory, **125**, pp. 34–44, 2018.

[21] R. C. Murray, C. Ophaswongse S. K. Agrawal. "Design of a Wheelchair Robot for Active Postural Support", ASME Journal of Mechanisms and Robotics, **11**(2), pp. 020911-1–9, 2019.

[22] M. Coste, K. M. Demdah. "Extra Modes of Operation and Self-motions in Manipulators Designed for Schoenfies Motion", Journal of Mechanism and Robotics, **7**, pp. 97–113, 2015.

[23] D. Chablat, X. Kong, C. Zhang. "Kinematics, Workspace and Singularity Analysis of a Multi-Mode Parallel Robot", Journal of Mechanism and Robotics, Proceedings of the ASME 2017 International Design Engineering Technical Conferences & Computers and Information in Engineering Conference IDETC/CIE 2017 August 69, 2017, Cleveland, Ohio, USA.

[24] X. Kong, Y. Jin, "Type Synthesis of 3-DOF multi-mode translational/spherical parallel mechanisms with lockable joints", Mechanism and Machine Theory, **96**(2), pp. 323–333, 2016.

[25] X. Kong, "Type synthesis of 3-DOF parallel manipulators with both a planar operation mode and a spatial translational operation mode", Journal of Mechanisms and Robotics, **5**(4), pp. 041015-1–8, 2013.

[26] J. Schadlbauer, M. Husty, S. Caro, P. Wenger, "Self-Motions of 3-RPS Manipulators", Frontiers of Mechanical Engineering, **8**(10), pp. 62–69, 2013.

[27] D. Chablat, E. Ottaviano, S. Venkateswaran, "Self-Motions conditions for a 3-PPPS parallel robot with delta-shaped base", Mechanism and Machine Theory, **135**, pp. 109–114, 2019.

[28] B. Khoshnevis. "Automated Construction by Contour Crafting - Related Robotics and Information Technologies, Automation in Construction,**13**(1), pp. 5–19. 2004.

[29] G. Cesaretti, E. Dini, X. De Kestelier, V. Colla, L. Pambaguian. "Building Components for An Outpost on The Lunar Soil by Means of A Novel 3D-Printing technology", Acta Astronautica, **93**, pp. 430–450, 2014.

[30] P. Krejcirik, D. Skaroupka, D. Palousek. "Free Directional Robotic Deposition-Influence of Overhang Printability", Modern Machinery Science Journal, **12**, pp. 2715–2721, 2018.

[31] X. Song, Y. Pan, Y. Chen. "Development of a Low-Cost Parallel Kinematic Machine for Multi-directional Additive Manufacturing", Journal of Mechanisms and Robotics, **137**, pp. 021005-1–14, 2015.

[32] Y. Gao, L. Wu, D-M .Yan, L. Nan. "Near Support-free Multi-directional 3D Printing via Global-Optimal Decomposition", Graphical Models, **104**, pp. 101034, 2019.